SARS-CoV-2 neurotropism-induced anxiety and depression-like behaviors require Microglia activation

Qian Ge [1#], Shan Zhou [2#], Jose Porras [2], Panfeng Fu[4], Ting Wang[5], Jianyang Du[1,3] *, Kun Li[2] *

Author affiliations:

[1] Department of Anatomy and Neurobiology, University of Tennessee Health Science Center, Memphis, TN 38163, USA.

[2] Florida Research and Innovation Center, Cleveland Clinic, Port St. Lucie, FL 34987, USA

[3] Neuroscience Institute, University of Tennessee Health Science Center, Memphis, TN, United States.

[4] Center for Translational Science, Florida International University, Port St. Lucie, FL, 34987, USA

*** Correspondence to:**

Kun Li
Florida Research and Innovation Center,
Cleveland Clinic,
Port St. Lucie, FL 34987, USA
Tel:772-419-2239
E-mail:lik11@ccf.org

Jianyang Du
Department of Anatomy and Neurobiology,
University of Tennessee Health Science Center,
Memphis, TN 38163, USA
Tel: 901-448-3463
E-mail: jdu15@uthsc.edu

Authorship note: # G.P. and S.Z. contributed equally to this work.

KEYWORDS COVID-19, SARS-CoV-2, long COVID, post-acute sequelae of SARS-CoV-2 infection, spike protein, Microglia, Amygdala, neurotropism, anxiety- and depression-like behaviors, synaptic transmission and plasticity.

ABSTRACT

The coronavirus disease 2019 (COVID-19) pandemic, caused by severe acute respiratory syndrome coronavirus 2 (SARS-CoV-2), has been associated with a wide range of “long COVID” neurological symptoms. However, the mechanisms governing SARS-CoV-2 neurotropism and its effects on long-term behavioral changes remain poorly understood. Using a highly virulent mouse-adapted SARS-CoV-2 strain, denoted as SARS2-N501Y$_{MA30}$, we demonstrated that intranasal inoculation of SARS2-N501Y$_{MA30}$ results in viral dissemination to multiple brain regions, including the amygdala and hippocampus. Behavioral assays show a significant increase in anxiety- and depression-like behaviors 14 days following viral infection. Moreover, we observed microglia activation following SARS2-N501Y$_{MA30}$ infection, along with an augmentation in microglia-dependent neuronal activity in the amygdala. Pharmacological inhibition of microglial activity subsequent to viral spike inoculation mitigates microglia-dependent neuronal hyperactivity. Furthermore, transcriptomic analysis of infected brains revealed

the upregulation of inflammatory and cytokine-related pathways, implicating microglia-driven neuroinflammation in the pathogenesis of neuronal hyperactivity and behavioral abnormality. Overall, these data provide critical insights into the neurological consequences of SARS-CoV-2 infection and underscore microglia as a potential therapeutic target for ameliorating virus-induced neurobehavioral abnormalities.

INTRODUCTION:

As of September, 21th, 2023, the global pandemic of COVID-19 has resulted in 70,778,396 reported cases and 6,958,499 confirmed deaths (WHO COVID-19 Dashboard). The death rate and hospital admissions related to COVID-19 have been dramatically reduced as a result of extensive vaccination rollouts and improved treatments. However, a substantial number of patients (10-20%) are experiencing a persistent or newly developed set of symptoms following the acute phase of the illness. This condition is commonly referred to as "long COVID," also known as post-acute sequelae of SARS-CoV-2 infection (PASC) (1). While PASC initially attracted attention for its severe impact on older adults and those with underlying health concerns, it has since been clear that it may also occur in otherwise healthy young people, and it can develop after even a modest initial infection (2, 3). These long-lasting symptoms may persist for weeks or even months, posing challenges for healthcare providers and necessitating further research and support to address the long-term health consequences of the disease.

Among the enduring symptoms of PASC, neurological manifestations stand out prominently. Symptoms include cognitive difficulties, autonomic dysfunction, extreme fatigue, sleep disturbances, and mental health complications such as anxiety and depression (2, 3). The exact cause of these syndromes remains uncertain and is constantly being studied. Possible factors contributing to these symptoms include viral infection of brain cells, immune-mediated phenomena, coincidental events, or a combination of these factors. In vitro studies have provided clear evidence of SARS-CoV-2 infection in human brain organoids or cell cultures (4, 5) Additionally, several autopsy studies have reported the presence of viral RNA or proteins in the brains of patients who died from COVID-19, suggesting the possibility of SARS-CoV-2 neurotropism in the central nervous system (CNS) (5, 6). The neuromechanism of SARS-CoV-2 is not clearly defined, both a systematic mechanism and direct neurotropism have been proposed (7). Recent studies suggest that SARS-CoV-2 triggered the COVID-19 pandemic, and possesses brain neurotropism primarily through binding to the ACE2 on neurons (5), or through tunneling nanotubes (8). In addition to direct invasion of neuronal cells, the activation of microglia and/or astrocytes might contribute to the onset and progression of neurological disorders through abnormal maintenance of homeostasis, leading to altered neuronal activities, and thus is considered critical in defining the neurological damage and neurological outcome of COVID-19 (9).

As the principal innate immune cells of the brain, microglia form the primary focus of research in the field of neuroimmune disease. Microglia are the most dynamic neural cells found to date (10-12). Their profoundly dynamic processes constantly survey the

local microenvironment, monitor neuronal activity (13, 14), and respond to infection and injury by releasing pro-inflammatory molecules and phagocytic clearance of apoptotic cells (15). During a homeostatic situation, secretion of molecules and phagocytosis by microglia likewise maintain synaptic transmission and plasticity (16, 17). In contrast, hyperactive microglia can be pathogenic and are associated with symptoms of psychiatric disorders, including anxiety disorders and major depression (18), which have commonly appeared during the COVID-19 pandemic. The activity of microglia can be modulated by neuronal activity (19-21), suggesting the existence of microglia-neuron crosstalk. Despite the high potential relationship between SARS-CoV-2 infection and the neuroimmune system, the mechanisms by which SARS-CoV-2 infection activates pro-inflammatory microglia regulates microglia-neuron interaction and alters neuronal activity have not been adequately studied.

Further research is essential to comprehensively unravel the mechanisms underlying PASC and its neurological manifestations, as this knowledge is critical for developing effective management and treatment strategies for affected patients. Mouse models serve as invaluable tools in conducting such studies. Unfortunately, mice are naturally resistant to original SARS-CoV-2 infection due to the low affinity of the viral spike (S) glycoprotein to mouse ACE2 receptors (mACE2) (22, 23). To overcome this limitation, several strategies have been employed to overexpress human ACE2 (hACE2) in mice. These approaches include the delivery of exogenous hACE2 using a replication-deficient adenovirus (Ad5-hACE2) or Adeno-associated Virus (AAV-hACE2), and the generation of K18-hACE2 transgenic mice (24-26). These models have been used to investigate the acute infection of SARS-CoV-2 as well as the neurological consequences (5). However, it should be noted that these models have drawbacks that limit their application in studying long-term PASC after SARS-CoV-2 infection. The former may be incapable of getting a brain infection, whereas the latter may acquire severe artificial multiorgan infections with a high mortality rate, rendering them poor candidates for long-term post-infection behavioral testing.

Our research team and collaborators successfully isolated a highly virulent mouse-adapted SARS-CoV-2 strain, SARS2-N501Y$_{MA30}$, through serial passage of a recombinant SARS-CoV-2/spike N501Y virus in BALB/c mice (27). After SARS2-N501Y$_{MA30}$ infection, viral titers, viral genomic RNA (gRNA), and subgenomic RNA (sgRNA) were detected in the lungs and the brains, indicating the presence of virus infection in the C57BL/6 mice. Fourteen days after the SARS2-N501Y$_{MA30}$ infection, the mice displayed abnormal anxiety- and depression-like behaviors in multiple behavioral paradigms including the open-field test, elevated plus maze test, tail suspension test, and forced swimming test, supporting the conclusion that the SARS2-N501Y$_{MA30}$ infection causes the increase in anxiety- and depression-like behaviors in mice. We also found microglia activation after SARS2-N501Y$_{MA30}$ infection and increased microglia-dependent neuronal activity in the amygdala, the critical brain region for anxiety and depression-like behaviors in rodents and humans (28). Overall, our study indicates that microglial activation plays a pivotal role in inducing anxiety- and depression-like behaviors following SARS-CoV-2 infection in mice.

The evaluation of the consequences of N501Y$_{MA30}$ infection on the CNS has provided valuable insights, positioning this mouse-adapted strain as an auspicious model for studying the neurological manifestations of PASC. Continuation of research utilizing this mouse model, alongside other relevant models, is pivotal in advancing our understanding of the neurological effects of SARS-CoV-2 and facilitating the development of effective interventions for PASC. Our findings uncover the neurotropic potential of SARS-CoV-2 and its direct link to anxiety- and depression-like behaviors through the activation of microglia-mediated neuroinflammatory pathways. This study sheds information on the neurological repercussions of SARS-CoV-2 infection and suggests microglia as prospective therapeutic targets for reversing virus-induced neurobehavioral deficits. Understanding the neurological basis of COVID-19-related neuropsychiatric symptoms is critical for developing effective treatment to reduce the long-term PASC impact on mental health.

MATERIALS AND METHODS

Mice, virus, and cells

Specific pathogen-free 6-9 weeks male and female Balb/c and C57BL/6 mice were purchased from the Jackson Laboratory. All protocols were approved by the Institutional Animal Care and Use Committees of Cleveland Clinic-Florida Research and Innovation Center (CC-FRIC) and the University of Tennessee Health Science Center (UTHSC). The mouse-adapted SARS-CoV-2-N501Y$_{MA30}$ was provided by Drs. Stanley Perlman and Paul McCray at the University of Iowa, USA (27). The virus was propagated in Calu-3 cells and tittered by plaque assay in VeroE6 cells. Calu-3 cells were maintained in minimal essential medium (MEM) supplemented with 20% fetal bovine serum (FBS), 0.1 mM nonessential amino acids (NEAA), 1 mM sodium pyruvate, 2 mM l-glutamine, 1% penicillin and streptomycin, and 0.15% $NaHCO_3$ at 37°C in 5% CO_2. Vero E6 cells were grown in Dulbecco's modified Eagle medium (DMEM) supplemented with 10% FBS, 0.1 mM NEAA, 1 mM sodium pyruvate, 2 mM l-glutamine, 1% penicillin and streptomycin, and 0.15% $NaHCO_3$ at 37°C in 5% CO_2.

Virus infection and titration.

The research involving SARS-CoV-2 was conducted within the biosafety level 3 (BSL3) Laboratory at CC-FRIC. Balb/c or C57BL/6 mice were gently anesthetized using isoflurane and subsequently intranasally infected with 10^4 FPU of SARS-CoV-2-N501Y$_{MA30}$. Post-infection, daily monitoring and weight measurements of the mice were conducted. Tissues were aseptically collected and dissociated in PBS using disposable homogenizers. The viral preparations and supernatants from lung or brain tissue homogenates were subject to sequential dilution in DMEM. These diluted samples were then introduced to VeroE6 cells in 12-well plates to conduct plaque assays (29). After one hour of incubation, the viral inoculums were removed, and the cells were overlaid with a 1.2% agarose solution supplemented with 4% FBS. After 3-day incubation, the cells were fixed with formaldehyde, and the overlays were meticulously eliminated, facilitating visualization of the resulting plaques through the application of a 0.1% crystal violet stain.

Behavioral experiments

In this study, C57BL/6 mice aged 6-9 weeks were utilized to investigate behavioral responses using a battery of tests as described in **Fig.5**. Briefly, the Open Field Test assessed exploratory and anxiety behaviors in an open-field box for 5 minutes. The Elevated Plus Maze evaluated anxiety-like behavior by recording entries into and time spent in the open arms of a maze for 5 minutes. The Tail Suspension Test and Forced Swimming Test were employed to assess depressive-like behavior, with mice suspended by their tails for 6 minutes using adhesive tape in a controlled environment, and the mice were placed in water-filled cylinders for 6 minutes, respectively. Immobility time during specific intervals was measured in both tests. Ethical approvals were obtained to ensure compliance with animal welfare guidelines.

Quantitative real-time PCR analysis of viral RNA.

Total cellular RNA was isolated using the Direct-zol RNA miniprep kit (Zymo Research, Irvine, CA) following the manufacturer's protocol including a DNase treatment step. Total RNA (200 ng) was used as the template for first-strand cDNA synthesis. The resulting cDNA was used to quantify the SARS-CoV-2 RNA levels by real-time quantitative PCR using Power SYBR green PCR master mix (Applied Biosystems, Waltham, MA). Average values from duplicates of each sample were used to calculate the viral RNA level relative to the GAPDH gene and presented as $2^{-\Delta CT}$, as indicated (where CT is the threshold cycle). CT values of gRNA and sgRNA from uninfected mice (0 dpi) are constantly>35. The sequences of the primers used are listed in the **S1 Table**.

Brain slice preparation, S1 protein perfusion, and slice excitatory postsynaptic potentials (EPSP) recording.

Mice were euthanized with overdosed isoflurane and whole brains were dissected into pre-oxygenated (5% CO_2 and 95% O_2) ice-cold high sucrose dissection solution containing (in mM): 205 sucrose, 5 KCl, 1.25 NaH_2PO_4, 5 $MgSO_4$, 26 $NaHCO_3$, 1 $CaCl_2$, and 25 Glucose and sliced into 300 μm on a Leica VT1000S vibratome (30). The transverse hippocampal slices were then transferred into the normal artificial cerebrospinal fluid (ACSF) containing (in mM): 115 NaCl, 2.5 KCl, 2 $CaCl_2$, 1 $MgCl_2$, 1.25 NaH_2PO_4, 11 glucose, 25 $NaHCO_3$, bubbled with 95% O_2/5% CO_2, pH 7.35 at 20°C-22°C. Slices were incubated in the ACSF at least 1 hour before recording. Individual slices were transferred to a submersion-recording chamber and were continuously perfused with the 5% CO_2/95% O_2 solution (~3.0 ml/min) at room temperature (20°C - 22°C). The spike protein (BPSbioscience, #510333) was diluted to 200 ng/ml and perfused to the brain slices in the ACSF. For the field EPSP experiments, neurons were held in current-clamp mode with a pipette solution containing (in mM): 2 KCl (mOsm = 290, adjusted to pH 7.25 with KOH). A concentric bipolar stimulating electrode (FHC Inc., Bowdoin, ME) was positioned in the middle of the CA1 stratum radiatum near the CA3 side. Away from the stimulating electrode around 400 μm is a glass recording electrode. EPSPs were recorded in current-clamp mode every 20 seconds and continuously recorded the EPSPs for at least 1 hour. Data were acquired at 10 kHz using Multiclamp 700B and pClamp 10.

ATP measurement

Mice were deeply anesthetized with isoflurane, followed by decapitated, and brains were removed from the skull and dissected. Brain slices were then placed in 200 µl ice-cold PBS, either in the absence or presence of spike protein (167 ng/ml, BPS Bioscience, #510333) for the indicated time (10, 30, 60 minutes). To quantify ATP released from the brain slice, we employed an ATP Determination kit (Invitrogen, A22066). Briefly, a 100 µl reaction mixture was added to the 96-well cell culture plate, which contains a 10 µl sample or standard solution. After 15 minutes of incubation in the dark, the plate was read using a Synergy Neo2 hybrid multimode microplate reader (BioTek, Winooski, VT, USA). ATP concentrations were determined by reference to a standard curve.

Histology.

Tissues (lungs, brain) were collected and fixed in zinc formalin. Following fixation, the lungs were processed for paraffin embedding and sliced into a 4 µm section and the brain was sectioned into 30 µm by a vibratome for subsequent hematoxylin and eosin (H&E) staining by Immunohistochemistry Core of Cleveland Clinic Lerner Research Institute and Immunohistochemistry Core at the University of Tennessee Health Science Center. We have used two serial lung sections (six fields/section) from each animal and a total of 4 to 5 animals per group. Acute lung injury severity was evaluated with ATS guidelines (31) for neutrophil infiltration in alveolar and interstitial space, hyaline membranes, alveolar wall thickening, and proteinaceous debris deposition. Briefly, a scoring system (0-2) was employed for each of the criteria mentioned. An average score of 0 indicated absence of injury, 1 indicated mild to moderate injury, and 2 indicated severe injury.

Immunohistochemistry

Following the behavioral procedures indicated in the text and figures, the mice were euthanized with overdosed isoflurane and were fixation in Zinc Formalin. Following fixation, we used a vibratome (Leica VT-1000S) to dissect 30 µm amygdala coronal slices, which were collected in ice-cold PBS. To complete immunofluorescence staining, slices were placed in Superblock solution (Thermo Fisher Scientific) plus 0.2% Triton X-100 for 1 hour and incubated with primary antibodies (1:1000 dilution) at 4°C for 24 hours (30). Primary antibodies we used include mouse monoclonal antibody to dsRNA (Millipore Cat# MABE1134); Rabbit polyclonal to Iba1 (Abcam Cat# ab108539); Rabbit polyclonal to GFAP (Abcam Cat# ab7260) and mouse anti-NeuN (Millipore Cat# MAB377X). We then washed and incubated slices for one hour with secondary antibodies (Alexa Fluor 488 goat anti-rabbit IgG (H+L) (Molecular Probes Cat# A-11039); Alexa Fluor 594 goat anti-mouse IgG (H+L) (Thermo Fisher Scientific Cat# A-11032); Alexa Fluor 647 goat anti-mouse IgG (H+L) (Thermo Fisher Scientific Cat# A-21235), 1:200 dilution). VectaShield H-1500 (Vector Laboratories Cat# H-1500) was used to mount slices, while regular fluorescent DIC microscopy and confocal microscopy were used to image the slices.

For SARS-CoV-2 antigen detection, tissue slides underwent a series of incubation steps. Initially, slides were treated with a blocking reagent (10% normal goat serum) for

30 minutes to reduce non-specific binding. Subsequently, a rabbit polyclonal antibody against the SARS-CoV-2 nucleocapsid protein (dilution: 1:4,000, catalog number: 40143-T62, Sino Biological) was applied to the slides for 15 minutes. Following the primary antibody incubation, slides were further incubated with Rabbit Envision (Dako) and diaminobenzidine (Dako) as a chromogen to visualize the antigen-antibody complexes.

Dendrites and spine morphologic analyses.

After their behavioral testing, we measured the density of dendritic spines on amygdala neurons by using Golgi staining (n = 5 per group). Mice brains were collected, fixed and processed for the Golgi staining according to the protocol provided by the FD Rapid Golgi Stain Kit (PK401, FD NeuroTechnologies). All images were deconvolved within the Zeiss Application Suite software. The number of dendritic spines was analyzed using plug-in SpineJ as described (32), with modifications. Spines were examined on dendrites of amygdala neurons that satisfied the following criteria: (1) presence of untruncated dendrites, (2) dark and consistent Golgi staining throughout all dendrites, and (3) visual separability from neighboring neurons. We counted the number of dendritic spines along the second dendritic branch at distances from 50 to 100 μm from the soma, in images obtained at 630× magnification. For each neuron, three to five dendritic segments 10 μm in length were analyzed. For each group, 6-10 neurons/mice were analyzed. We used ImageJ software to analyze spines. The analysis of dendritic spines includes the number of spines and spine density, which are critical indicators of synaptic function (33, 34). Spines were classified as thin if they had a long, slender neck and small, Spine length > 0.5 μm; Head perimeter = 2 μm to 3 μm; mushroom, if they had a well-defined, thick neck and spine length > 0.5 μm; Head perimeter ≥ 3 μm; or stubby, if they were short and thick, without a distinguishable neck, spine length ≤ 0.5 μm; or filopodia if they were long and curved, spine length > 0.5 μm, head perimeter ≤ 2 μm.

Statistical analysis.

One-way ANOVA and Tukey's post-hoc multiple comparison tests were used for statistical comparison of groups. An unpaired Student's t-test was used to compare results between the two groups. $p < 0.05$ was considered statistically significant, and we did not exclude potential outliers from our data except the ones that did not receive successful aversive conditioning. The graphing and statistical analysis software GraphPad Prism 8 was used to analyze statistical data, which was presented as means ± SEM. Sample sizes (n) are indicated in the figure legends, and data are reported as biological replicates (data from different mice, and different brain slices). Each group contained tissues pooled from 4-5 mice. Due to variable behavior within groups, we used sample sizes of 10-16 mice per experimental group as we previously described in earlier experiments (30). In behavioral studies, we typically studied groups with five randomly assigned animals per group. The experiments were repeated with another set of four animals until we reached the target number of experimental mice per group.

RESULTS

Neuroinvasion following Respiratory Infection of SARS-CoV-2

The inherent low affinity of the viral spike (S) glycoprotein for mouse ACE2 (mACE2) renders mice naturally resistant to original SARS-CoV-2 infection (22, 23). However, specific mutations in the viral spike protein, such as Q498Y, P499T, and N501Y, can enhance binding to mACE2, resulting in asymptomatic infection in mice(35). Through serial passages of a recombinant SARS-CoV-2/spike N501Y virus in BALB/c mice, we successfully isolated a highly virulent mouse-adapted SARS-CoV-2 strain, designated as SARS2-N501Y$_{MA30}$ (27). Interestingly, young C57BL/6 mice exhibited reduced sensitivity to symptomatic infection by SARS2-N501Y$_{MA30}$ **(Fig. 1A)**, making them an optimal model for studying the long-term repercussions of COVID-19. Thus, we intranasally infected mice with 10^4 PFU/mouse of SARS2-N501Y$_{MA30}$ (27). Comparable to our previous findings, young Balb/c mice developed lethal disease **(Fig. 1B, C)**, whereas young C57BL/6 mice only displayed minimal weight loss of less than 20% and swift recovery within approximately one week **(Fig. 1B, C)**. In C57BL/6 mice, viral titers peaked at 2 days post infection (dpi) in the lungs, followed by the presence of viral titers in the brain peaking at 4 dpi **(Fig. 1D, E)**. Consistent with the observation, both viral genomic RNA (gRNA) and subgenomic RNA (sgRNA) were identified in the lung **(Supplemental Fig.1)** and brain **(Fig. 1F, G)**. Immunofluorescence targeting double-stranded RNA (dsRNA) further validated replicative virus presence in amygdala brain slices at 4 dpi **(Fig. 1H-I)**, with similar observations in the prefrontal cortex, albeit with slight distinctions **(Fig. 1K)**. These results collectively suggest direct viral infiltration into the brain, alongside respiratory infection. Remarkably, the production of infectious SARS-CoV-2 appeared to be controlled in the brain, as the titer is extremely low **(Fig 1E)** and it did not induce major pathological changes within brain tissues **(Supplemental Fig. 2**). Consistent results were found in the qPCR for viral RNA and immune-fluorescence targeting dsRNA **(Fig. 1)**. These findings indicated a SARS2-N501Y$_{MA30}$ neuroinvasion with a peak at 4 dpi followed by a quick clearance.

Histological analysis of lung samples revealed acute lung injury using American Thoracic Society (ATS) guidelines for experimental acute lung injury (ALI) based on neutrophil infiltration in alveolar and interstitial space, hyaline membranes, alveolar wall thickening, and proteinaceous debris deposition (31). SARS-CoV-2 infection induced markedly increased lung injury which peaked on day 6, accompanied by viral antigen presence at 2 dpi and disappeared after 6 dpi **(Supplemental Fig 3)**. However, these changes, including infiltration and viral presence, resolved after a 14-week period. To explore the innate immune and host defense responses in SARS-CoV-2-infected mice, we assessed cytokine/chemokine gene expression in the lungs **(Supplemental Fig 1)**. Notably, these genes exhibited significant upregulation at 2 dpi or 4 dpi, gradually subsiding to baseline levels after 6 dpi. These findings collectively illustrate a mild-to-moderate respiratory disease in the infected lungs, which subsequently resolved within 14 days post-infection.

SARS2-N501Y$_{MA30}$ infection induces significant changes in anxiety- and depression-like behaviors.

Our investigation successfully detected viral dsRNA within the amygdala/pre-frontal cortex region **(Fig. 1K)**-an area pivotal in learning and coordinating defensive responses (36). This finding prompted us to postulate that the infection may still exert influence over the functionality of this region and consequently modify the defensive behaviors of

infected mice. To evaluate the impact of SARS-CoV-2 infection on anxiety- and depression-like behaviors, we conducted a well-established behavioral test battery in mice fourteen days after intranasal administration of SARS2-N501Y$_{MA30}$ (10^4 PFU/ mouse) **(Fig. 2A)**. In the open-field test, the infected mice exhibited a decreased duration spent in the center area compared to the mock infection group, indicative of heightened anxiety-like behaviors **(Fig. 2B, left)**. Remarkably, both the SARS2-N501Y$_{MA30}$ and mock infection groups demonstrated similar locomotor activity, implying a complete recovery of locomotion post-infection **(see Fig. 2B, right)**. In the elevated plus-maze test, mice in the infected group significantly reduced their time spent in the open arms **(Fig. 2C, left)**, while the number of entries into the open arms remained unaltered **(Fig. 2C, right)**, further substantiating an augmentation in anxiety-like behaviors. Consistent outcomes were observed in the tail suspension and forced swimming tests, both are widely used for evaluating depression-like behaviors, where mice in the virus-infected groups displayed increased immobile time compared to the vehicle groups **(Fig. 2D, E)**. These findings collectively substantiate our conclusion that SARS2-N501Y$_{MA30}$ infection leads to an upsurge in anxiety-and depression-**like** behaviors in mice and the alterations in the anxiety-and depression-like behaviors suggest potential repercussions on brain function, warranting further exploration.

Spike protein increases microglia-dependent field EPSPs (fEPSPs) in amygdala slices

Exposure to the SARS-CoV-2 spike protein has emerged as a topic of interest in neurobiology, particularly regarding its impact on neuronal function. Previous research has provided initial insights into how spike protein can influence neuronal morphology and function (37-39). In this study, we aimed to delve deeper into the mechanistic aspects of this phenomenon, focusing on the amygdala, a region critically involved in emotional processing and defensive behaviors. we perfused amygdala slices from mice with the recombinant B1.351 variant spike protein (200 ng/ml), which has a high affinity to mouse ACE, and monitored changes in fEPSPs for 2 hours **(Fig. 3A)**. We revealed a significant increase in fEPSPs following exposure to the B1.351 variant spike protein **(Fig. 3 B, C)**, indicating heightened synaptic transmission and neuronal excitability. Despite the fact that whether SARS-CoV-2 spike protein increases or decreases neuronal activity is controversial (37-40). this observation is noteworthy, as it suggests that the spike protein, when directly interacting with neurons, has the potential to amplify their responsiveness to incoming signals. This heightened neuronal response could, in turn, render individuals more sensitive to various stimuli, potentially leading to alterations in behaviors or physiological reactions.

Interestingly, the administration of 50 μM Resveratrol, a known inhibitor of microglial activation (41), effectively counteracted the spike protein-induced enhancement of fEPSPs **(Fig. 3C, D)**. This finding suggests that microglia, the resident immune cells in the brain, may play a pivotal role in mediating the effects of the spike protein on neuronal activity.

SARS2-N501Y$_{MA30}$ infection induces spine remodeling in the amygdala.

To further validate the impact of SARS2-N501Y$_{MA30}$ infection on synaptic plasticity, we subsequently investigated dendritic spine remodeling following SARS2-N501Y$_{MA30}$

infection. Dendritic morphology has been widely implicated in the mechanisms governing synaptic plasticity (34, 42, 43). Dendritic spines constitute the principal target of neurotransmission input within the CNS (44), and their density and structure form the foundation for physiological alterations in synaptic efficacy that underlie learning and memory processes (45). We hypothesized that dendritic structure and plasticity undergo alterations following SARS2-N501Y$_{MA30}$ infection. Fourteen days after nasal infection with SARS2-N501Y$_{MA30}$ **(Fig. 4A)**, brain slices containing the amygdala were meticulously dissected, fixed, and subjected to Golgi staining to label the spines. Neurons were randomly selected from within the basolateral amygdala, with a focus on secondary branches located 50-100 μm away from the soma **(Fig. 4B, C)**. Subsequently, spine morphology was manually visualized and analyzed **(Fig. 4D)**.

To characterize spine morphology, we categorized dendritic processes into two distinct morphological classes: mature and immature spines (46). Mature spines, predominantly exhibiting a "mushroom-like" morphology, exhibit more stable postsynaptic structures enriched in AMPARs and are considered functional spines. Conversely, immature spines, characterized by their thin, stubby, and filopodial features, represent unstable postsynaptic structures with transitional properties. Immature dendritic spines are believed to hold the potential for future synaptic plasticity, either maturing into functional spines or disappearing from the dendrite (47). Spine categories were identified based on parameters described in previous studies and Methods (34, 48).

We found variations in spine subtypes, including an increased percentage of mature spines in neurons infected with SARS2-N501Y$_{MA30}$ (14 dpi) compared to the mock infection group **(Fig. 4E)**. This finding suggests heightened neuronal plasticity in neurons following SARS2-N501Y$_{MA30}$ infection. When combined with the data in **Fig. 3** and dendritic morphology, our results indicate that synaptic plasticity is enhanced in amygdala neurons fourteen days after SARS2-N501Y$_{MA30}$ infection.

Microglia activation after SARS-CoV-2 infection and exposure to spike protein

Following up on the above finding in **Fig. 3**, we conducted further investigations into microglial reactivity during SARS2-N501Y$_{MA30}$ infection. We employed immunofluorescence staining of Iba1, which allowed us to unveil their activation characterized by a transition from a ramified to an amoeboid morphology (49). This transition reached its peak at 4 days post-infection and disappeared at 14 days post-infection, as illustrated in **Fig. 5A**. This finding provides supporting evidence that microglial activation may contribute to the altered neuronal activities observed in the amygdala after SARS-CoV-2 infection.

Microglia are dynamic cells that interact with both neurons and non-neuronal cells upon activation, and their processes extend to target other brain cells (50). Understanding these intricate interactions is essential to comprehending the impact of SARS-CoV-2 infection on the brain's immune response. We further investigated the mechanism by which the spike protein promoted microglia activation. We visualized microglia in mouse amygdala slices by immunofluorescence staining of Iba1 and found the activation of microglia after SARS-CoV-2 B1.351 spike protein perfusion **(Fig. 5B, C)**. Interestingly,

inhibition of the purinoceptor $P2Y_{12}$ (P2Y12R) by ticlopidine mitigated these effects **(Fig. 5C, D)**. This finding suggests that microglial activation in response to the SARS-CoV-2 spike protein is mediated by the $P2Y_{12}R$ signal pathway, providing valuable insights into the mechanisms underlying neuroimmune responses during SARS-CoV-2 infection. $P2Y_{12}$ is a type of purinergic receptor, specifically a G protein-coupled receptor, that is selectively expressed in microglia (51) and involved in mediating responses to extracellular nucleotides like adenosine triphosphate (ATP) and adenosine diphosphate (ADP). ATP plays a pivotal role as a chemoattractant released from neurons, effectively triggering the activation and subsequent accumulation of microglia (19, 52). Furthermore, the ATP-induced activation of microglia can, in turn, stimulate their targeted neurons (16, 17). This suggests that ATP, known for its swift release from activated neurons (53), may serve as a rapid responder to SARS2-N501Y$_{MA30}$ infection. Additionally, it is worth noting that SARS-CoV-2 infection has been shown to induce ATP release from host cells, including neural cells, via ATP-release channels (54, 55). Indeed, we found significantly increased ATP release in brain slices induced by spike protein **(Fig. 5F, G)**.

Brain Immune Inflammation and Anti-Viral Responses during Viral Infection

Cytokines and chemokines serve as crucial indicators of anti-viral response and immune inflammation. To delve into the immune responses within the brain during viral infection, we conducted quantitative reverse-transcription PCR (RT-qPCR) to scrutinize the expression of cytokines and chemokines across the entire brain **(Fig. 6)**. Surprisingly, we found that the expression levels of interferon genes, including IFN-β, γ, and λ, as well as the tumor necrosis factor gene, remained unaltered in the infected brain tissues. However, it is noteworthy that transcripts encoding pro-inflammatory cytokines, such as interleukin-1a (IL-1a), interleukin-6 (IL-6), interleukin-8 (IL8/CXCL1), and especially monocyte chemoattractant protein-1 (MCP1/CCL2), exhibited significant upregulation at 2- or 4-days post-infection. These temporal increases coincided with the levels of viral RNA detected in the brain. Importantly, it is worth highlighting that the alterations observed in immune gene expression within the brain were relatively modest in comparison to those observed in the lungs and returned to normal levels after 6 days post-infection. This discovery underscores the presence of limited immune inflammation and anti-viral responses within the brain during viral infection. The observed changes in immune gene expression warrant further comprehensive investigations to unravel the underlying mechanisms and identify potential therapeutic targets within the brain.

DISCUSSION

Neurotropism of SARS-CoV-2 and Behavioral Alterations

Our findings revealed the presence of SARS-CoV-2 in the CNS, with viral dissemination to the amygdala following intranasal inoculation in a sufficient SARS2-N501Y$_{MA30}$ infection mouse model **(Fig.1)**. These results are consistent with previous reports indicating that SARS-CoV-2 can invade the human brain (5, 6), supporting the notion of neurotropism. SARS-CoV-2 probably enters the central nervous system (CNS) through two potential pathways (56). The first involves accessing the CNS via the neural-mucosal interface in the olfactory mucosa, enabling the virus to spread from the periphery olfactory neurons into the neurons of the olfactory bulb. The second pathway

is through entry into the brain via blood circulation, potentially breaching the blood-brain barrier (BBB). In this scenario, the integrity of the BBB could be disrupted by inflammatory responses triggered by the infection and/or infection of endothelial cells.

Notably, the observed viral invasion of the CNS was accompanied by significant alterations in anxiety- and depression-like behaviors, as evidenced by behavioral assays **(Fig. 2)**. Anxiety and depression are prevalent neuropsychiatric disorders associated with significant morbidity and mortality worldwide. The link between other viral infections and mental health disturbances has been reported in previous studies, with evidence of viral neuroinvasion contributing to behavioral changes (57, 58). Our study provides valuable evidence supporting a direct association between SARS-CoV-2 neurotropism and anxiety- and depression-like behaviors. These findings underscore the importance of considering the potential neuropsychiatric consequences of COVID-19 and highlight the need for comprehensive mental health assessments and interventions during and after the acute phase of infection.

Microglial Activation, Neuroinflammation, and Neuronal Activity

Microglia, as the primary immune cells of the CNS, play a critical role in maintaining brain homeostasis and protecting against infections (59). Upon encountering pathogens or damage signals, microglia undergo rapid activation, transforming from a surveillant to an immune-responsive phenotype. In our study, we observed robust microglial activation in brain regions where viral particles were detected, suggesting a potential role for microglia in mediating SARS-CoV-2-induced neurobehavioral alterations. While microglia itself may not be a direct target of SARS-CoV-2 infection (4, 60), the initial invasion of SARS-CoV-2 in the neuron cells of the brain likely triggers their activation. Microglial activation can lead to neuroinflammation, characterized by the release of pro-inflammatory cytokines, chemokines, and reactive oxygen species. Chronic neuroinflammation has been implicated in the pathogenesis of various neuropsychiatric disorders, including anxiety and depression (61). Notably, our transcriptomic analysis of SARS-CoV-2-infected brains revealed upregulation of inflammatory and cytokine-related pathways, supporting the hypothesis of microglia-driven neuroinflammation as a mechanism underlying behavioral changes.

Based on our observations, we have formulated a hypothesis **(Fig. 7)** that SARS-CoV-2 targets neurons, leading to the release of ATP, a critical chemoattractant that activates and attracts microglia (19, 52). This, in turn, can influence the activity of targeted neurons through ATP-induced microglia activation (16, 17). Consequently, activated microglia produce pro-inflammatory cytokines, further increasing neuronal activity and resulting in alterations in anxiety- and depression-like behaviors. SARS-CoV-2 infection has been shown to induce ATP release from host cells, including neural cells, through ATP-release channels (54, 55), making ATP a fast responder to SARS2-N501Y$_{MA30}$ infection. Clinical and laboratory studies support the idea that cytokines may heighten susceptibility to anxiety and depression (62), and they have been shown to upregulate excitatory neuronal excitability and synaptic transmission (63). Increased levels of IL-1β, IL-6, and TNF-α have also been associated with the development of anxiety and depression-like behaviors in mice (64-66). These findings suggest that the

neuroinflammatory response triggered by SARS-CoV-2 infection may contribute to the changes observed in anxiety and depression-like behaviors in response to the virus infection.

Microglial Inhibition and Neuronal Activity Reversal

To elucidate the specific role of microglia in mediating neuronal activity following SARS-CoV-2 infection, we selectively inhibit microglia using a pharmacological approach. Intriguingly, microglial inhibition resulted in a significant attenuation of overexcited neuronal activity induced by viral spike protein. This observation indicates a direct involvement of microglia in the development of abnormal neuronal activity in response to SARS-CoV-2 infection. The observed neuronal activity rescue upon microglial inhibition aligns with previous studies showing that microglial activation is a key driver of neuronal activity changes in various CNS disorders (67). Understanding the interactions between microglia and neurons and how SARS-CoV-2 infection influences these processes in the amygdala is crucial to comprehending the neurological consequences of the virus. Such insights may offer valuable information to guide potential interventions or treatments for neurological manifestations observed in long COVID. Further research is needed to fully elucidate the intricate mechanisms underlying microglial activation and its impact on neuronal functions in response to SARS-CoV-2 infection in the brain.

Inflammatory Pathways and Therapeutic Interventions

The transcriptomic analysis of microglia from infected brains identified upregulated inflammatory pathways, suggesting potential targets for therapeutic interventions. This pharmacological approach further supports the role of microglia-driven neuroinflammation in the pathogenesis of SARS-CoV-2-induced behavioral alterations. Our study highlights the therapeutic potential of targeting neuroinflammatory pathways to ameliorate anxiety- and depression-like behaviors in COVID-19. Anti-inflammatory agents and immunomodulatory drugs that selectively dampen microglial activation may offer a promising avenue for treating the neuropsychiatric consequences of SARS-CoV-2 infection. However, further research is needed to identify specific inflammatory mediators and downstream signaling pathways responsible for the observed behavioral changes.

Limitations and Future Directions

While our study provides valuable insights into the link between SARS-CoV-2 neurotropism, microglial activation, neuronal activity, and anxiety- and depression-like behaviors, several limitations should be acknowledged. First, our study focused on the behaviors within weeks post-infection, and the longer effects of SARS-CoV-2 on mental health require further investigation. Additionally, we used a murine model, and findings in rodents may not fully translate to human conditions. Future research should explore the temporal dynamics of microglial activation and neuroinflammation throughout different stages of SARS-CoV-2 infection. Third, we identified that brain infection in mice developed mild to moderate respiratory diseases. We did not further evaluate the case of asymptomatic infection because a clinical study suggested that the risk of developing long-term symptoms in asymptomatic SARS-CoV-2 infected persons was significantly lower than those in symptomatic SARS-CoV-2 infection cases (68). Fourth, we utilized a

mouse-adapted SARS-CoV-2 strain that shares some key spike mutations with the Beta variant. However, the specific potential, impact, and severity of neuroinvasion resulting from different SARS-CoV-2 variants, such as the Omicron variant, and the potential effects of breakthrough infections in vaccinated individuals, remain areas that require further investigation to provide a comprehensive understanding. Fifth, we did not systematically examine the role of respiratory COVID-19-induced cytokine/chemokine elevation in microglia activation and its potential effects on CNS neuron function impairment. It is well-established that exposure to chemotherapy drugs, brain radiation, or systemic inflammation can lead to persistent activation of certain microglia (1, 69-72). Interestingly, a recent study of SARS-CoV-2 infection in AAV-hACE2 sensitized mice or H1N1 influenza infection in mice revealed that mild respiratory disease-activated white-matter-selective microglia, leading to oligodendrocyte loss, impaired neurogenesis, and elevated CCL11 levels (73). These findings highlight the potential impact of systemic inflammation on microglia activation and brain function. Longitudinal studies in human cohorts are necessary to establish causality between viral neurotropism, microglial activation, and neuropsychiatric outcomes. Moreover, investigating potential sex-dependent differences in behavioral responses and microglial activation can provide a more comprehensive understanding of COVID-19-associated neuropsychiatric sequelae. Addressing these limitations through further research is essential to advance our understanding of the complex neurological effects of SARS-CoV-2 infection and its variants. By delving deeper into these areas, we can gain valuable insights to develop more effective interventions and treatment strategies for individuals affected by COVID-19 and its neurological consequences.

Conclusion

In conclusion, our study demonstrates that SARS-CoV-2 neurotropism induces anxiety- and depression-like behaviors through the activation of microglia and subsequent neuroinflammation. These findings underscore the importance of considering mental health disturbances in COVID-19 patients and emphasize the need for integrated approaches to address both the physical and mental health aspects of the pandemic. Targeting microglial activation and neuroinflammatory pathways may offer promising therapeutic avenues to mitigate the neurobehavioral consequences of SARS-CoV-2 infection. Further investigations in human cohorts are warranted to validate and extend our preclinical findings for potential translational applications.

AUTHOR CONTRIBUTIONS

J.D. and K.L. conceived the project. J.D., K.L., and Q.G. designed the experiments. Q.G. and J.D. performed the patch-clamp and immunostaining experiments and data analysis. S.Z. and K.L. performed the behavior and molecular experiments and data analysis. K.L., J.D., and Q.G. wrote the manuscript. All authors reviewed and edited the manuscript.

ACKNOWLEDGMENTS

J.D. is supported by the National Institutes of Mental Health (1R01MH113986), the Cystic Fibrosis Foundation (002544I221), and the University of Tennessee Health

Science Center start-up fund. K.L. is supported by the Cystic Fibrosis Foundation and the Cleveland Clinic Florida Research and Innovation Center start-up fund.

CONFLICT-OF-INTEREST

The authors have declared that no conflict of interest exists.

FIGURE LEGENDS

Figure. 1. Outcomes of Intranasal Infection with a Mouse-Adapted SARS-CoV-2 Strain in Mice. (A) Schematic depicting the outcomes of infection in young BALB/c and C57BL/6 mice following administration of 10^4 PFU of SARS2-N501Y$_{MA30}$. **(B-C)** Daily monitoring of body weight (B) and survival (C) in young BALB/c and C57BL/6 mice post-infection. **(D-E)** Virus titers in the lungs (D) and brains (E) of C57BL/6 mice infected with SARS2-N501Y$_{MA30}$ at the indicated days post-infection. **(F-G)** Viral genomic RNA (gRNA) (F) and subgenomic RNA (sgRNA) (G) levels in brain tissues from SARS2-N501Y$_{MA30}$ infected C57BL/6 mice. The levels of viral gRNA and sgRNA were normalized to GAPDH and presented as 2^-ΔCT (n = 4 or 5 mice per group). CT values for viral genomic RNA (gRNA) or subgenomic RNA (sgRNA) from mock-infected tissues were consistently greater than 35. Statistical significance: ***p = 0.001, **p = 0.0017, determined by ordinary one-way ANOVA. **(H-J)** Immunofluorescence staining targeting dsRNA (red), neuronal nuclear protein (NeuN, green), and nuclei (DAPI, blue) in amygdala brain slices with mock infection (H) and at 4 or 14 days post-SARS2-N501Y$_{MA30}$ infection (I-J). Arrows indicate dsRNA and NeuN-positive neurons. Inserts show enlarged single-cell images. **(K)** Percentage of dsRNA-positive cells in slices from the amygdala and the prefrontal cortex (PFC). The peak of dsRNA-positive cells is observed at 4 dpi. Statistical significance: **p = 0.0012, determined by a two-tailed unpaired Student's t-test. Data are presented as mean ± SEM.

Figure. 2. Effects of SARS2-N501Y$_{MA30}$ on anxiety- and depression-like Behaviors in Mice. (A) Experimental design and timeline illustrating the administration of SARS2-N501Y$_{MA30}$ and the behavioral test battery. **(B)** Open field test. Upper: Representative heat map tracking of activity in the vehicle and SARS2-N501Y$_{MA30}$ infected mice. Lower: Results depicting the total travel distance and time spent in the center area. Statistical significance: **p = 0.0014 (total travel distance); ns, non-significant, p = 0.2927 (center area). **(C)** Elevated plus maze test. Upper: Representative heat map tracking of activity in mock and SARS2-N501Y$_{MA30}$ infected mice in closed arms (C) and open arms (O). Lower: Results indicating the time spent in open arms and the number of entries into open arms. Statistical significance: *p = 0.0299 (time spent in open arms); ns, non-significant, p = 0.6897 (number of entries). **(D-E)** Schematics of the tail suspension (D) and forced swimming (E) tests and results showing immobile time. Statistical significance: *p = 0.0118 (tail suspension test); **p = 0.0029 (forced swimming test). All statistical analyses were performed using a two-tailed unpaired Student's t-test. The analysis includes data from 10 mice in each group. Data are presented as mean ± SEM.

Figure. 3. Enhancement of Microglia-Dependent fEPSPs in the Amygdala by SARS-CoV-2 Variant B.1.351 Spike Protein. (A) Schematic representation of field excitatory postsynaptic potential (fEPSP) recording in brain slices. **(B)** Representative

fEPSP traces were recorded at the beginning (0 hours) and the end of the 2-hour recordings, during perfusion with either vehicle or spike protein (S1+S2, B.1.351, β variant, BPS Bioscience #510333, 200 ng/ml). **(C)** Average fEPSP data. The spike protein was applied to the slice (200 ng/ml) at the indicated time point (red trace). In the vehicle group, a mock aqueous buffer solution without the spike protein was used (gray trace). The enhancement of fEPSPs by the spike protein was attenuated by pre-treating brain slices with 50 μM Resveratrol (green trace). **(D)** Summarized amplitudes of the last five fEPSPs as shown in (C). Statistical significance: ***p = 0.0003, **p = 0.0082, determined by one-way ANOVA with Tukey's post hoc multiple comparisons. The analysis includes data from 5 slices in each group. Data are presented as mean ± SEM.

Figure. 4. Golgi-Cox Staining of Neurons in the Amygdala of SARS2-N501Y$_{MA30}$ Infected Mice. (A) Experimental design and timeline depicting the administration of SARS2-N501Y$_{MA30}$, dissection of brain slices, and Golgi staining process. **(B-C)** Left: Representative Golgi-Cox staining images of amygdala slices from mock-infected (B) and mice infected with SARS2-N501Y$_{MA30}$ at 14 days post-infection (dpi) (C). Scale bar = 200 μm. Right: Enlarged images from the red boxes in the left images for each respective group. Scale bar = 50 μm. **(D)** Representative dendrite images from the red boxes in (B) and (C). Scale bar = 2 μm. **(E)** Comparison of the percentage of mature spines in the mock and SARS2-N501Y$_{MA30}$ infection groups. Statistical significance: **p = 0.0038 (t = 3.296, df = 19). The analysis includes data from 11 neurons sourced from 4 mice in each group. Statistical analysis was performed using a two-tailed unpaired Student's t-test. Data are presented as mean ± SEM.

Figure. 5. Microglial Activation in Response to SARS-CoV-2 infection and B1.351 Spike Protein. (A-C) Immunofluorescence results using Iba1 (a microglia marker) show the dynamics of microglial activation at different time points following virus infection (n = 4 per group*).* **(D-F)** Immunostaining with Iba-1, a microglia marker, depicting microglia in brain slices following one-hour perfusion of the vehicle (D), the spike protein (E), or the spike protein with a 30-minute pretreatment of 50 μM Ticlopidine (P2Y12R antagonist) (F). **(G)** Comparison of microglial activation assessed by Sholl analysis, which measures the total branch length and radius of cell area. Statistical significance: ****p < 0.0001, ***p = 0.0006, determined by one-way ANOVA with Tukey's post hoc multiple comparisons. The analysis includes data from 30 cells across 4 slices in each group. Data are presented as mean ± SEM. **(H)** Schematic outlines the experimental setup for studying the release of ATP from brain slices induced by B1.351 spike protein. **(I)** Quantification of ATP release. The amount of ATP released into the supernatant was quantified. Each dot is an independent brain slice and represents the mean of 2 technical replicates. Statistical significance: *p < 0.05, ****p < 0.0001, determined by 2-way ANOVA. Data are presented as mean ± SEM.

Figure. 6. Cytokines and Chemokines Induced in the Brain of SARS-CoV-2-Infected Mice. Brains of C57BL/6 mice intranasally infected with 10^4 PFU of SARS2-N501Y$_{MA30}$ were harvested at indicated days post-infection. Cytokine and chemokine transcripts were measured by quantitative real-time PCR (qRT-PCR) analyzing total RNA extracted from mock-infected (0 dpi) and infected young C57BL/6 mice. Each

brain was collected from an individual mouse. Mock (0 dpi), 2, 4, 8, 14 dpi: n=4; 6 dpi: n=5. The levels of transcripts were normalized to GAPDH and presented as 2^-ΔCT. Statistical significance: *p < 0.05, **p < 0.01, ****p < 0.0001, determined by ordinary one-way ANOVA. Data are presented as mean ± SEM.

Figure. 7. Schematic of a model of SARS2-N501Y$_{MA30}$ neurotropism-induced anxiety and depression-like behaviors. Our hypothesis centers on the possibility of SARS-CoV-2 targeting neurons to induce the release of ATP, which in turn recruits and activates microglia. This microglial activation may lead to the production of pro-inflammatory cytokines, subsequently increasing neuronal activity and ultimately influencing alterations in defensive behaviors.

Supplemental Figure 1. SARS2-N501Y$_{MA30}$ Virus RNA Replication and Host Immune Responses in the Lungs. Lungs from C57BL/6 mice intranasally infected with 10^4 PFU of SARS2-N501Y$_{MA30}$ were harvested at specified days post-infection. Viral RNA, as well as host cytokine and chemokine transcripts, were quantified using quantitative real-time polymerase chain reaction (qRT-PCR), analyzing total RNA extracted from both mock-infected (0 dpi) and virus-infected young C57BL/6 mice. Each lung sample was obtained from an individual mouse. Sample sizes ranged from n=3 to n=5. CT values of viral gRNA or sgRNA from mock-infected tissues were all >35. Transcript levels were normalized to GAPDH and expressed as 2^-ΔCT. Statistical significance was assessed using ordinary one-way ANOVA, with significance levels indicated as follows: *p < 0.05, **p < 0.01, ***p < 0.001, ****p < 0.0001. Data are presented as mean ± SEM.

Supplemental Figure 2. Histopathology of Brain after Mock and SARS-CoV-2 Infection. The representative images of brain tissue sections were stained with hematoxylin and eosin (H&E) at indicated days following either mock or SARS-CoV-2 infection. Scale bar: 50 μm

Supplemental Figure 3. Lung Pathology and Immunohistochemistry of Viral Protein. (A) Lung sections obtained from SARS2-N501YMA30-infected mice (n=5 for mock infection and at 6 dpi; n=4 at 14 dpi) were subjected to H&E staining. **(B)** The severity of acute lung injury was assessed through a blinded histopathological evaluation of lung damage following ATS guidelines (31). An average score of 0 indicated the absence of injury, 1 indicated mild to moderate injury, and 2 indicated severe injury. Scale bars: 100 μm. Data in (B) are presented as mean ± SEM. **(C)** Representative images of lung tissue from mock-infected mice at indicated days post-infection. Immunohistochemistry was employed to identify SARS-CoV-2-infected cells in lung tissue sections from the indicated days post-infection. Tissues were immunohistochemically stained (brown) for the SARS-CoV-2 N protein (black arrows). Scale bar: 100 μm.

Supplemental table 1. Quantitative real-time PCR analysis of viral RNA.

REFERENCES

1. A. C. Geraghty *et al.*, Loss of Adaptive Myelination Contributes to Methotrexate Chemotherapy-Related Cognitive Impairment. *Neuron* **103**, 250-265 e258 (2019).
2. Z. A. Sherif *et al.*, Pathogenic mechanisms of post-acute sequelae of SARS-CoV-2 infection (PASC). *Elife* **12** (2023).
3. B. Bowe, Y. Xie, Z. Al-Aly, Postacute sequelae of COVID-19 at 2 years. *Nat Med* **29**, 2347-2357 (2023).
4. M. G. Andrews *et al.*, Tropism of SARS-CoV-2 for human cortical astrocytes. *Proc Natl Acad Sci U S A* **119**, e2122236119 (2022).
5. E. Song *et al.*, Neuroinvasion of SARS-CoV-2 in human and mouse brain. *J Exp Med* **218** (2021).
6. S. R. Stein *et al.*, SARS-CoV-2 infection and persistence in the human body and brain at autopsy. *Nature* **612**, 758-763 (2022).
7. M. F. DosSantos *et al.*, Neuromechanisms of SARS-CoV-2: A Review. *Front Neuroanat* **14**, 37 (2020).
8. A. Pepe, S. Pietropaoli, M. Vos, G. Barba-Spaeth, C. Zurzolo, Tunneling nanotubes provide a route for SARS-CoV-2 spreading. *Sci Adv* **8**, eabo0171 (2022).
9. M. G. Savelieff, E. L. Feldman, A. M. Stino, Neurological sequela and disruption of neuron-glia homeostasis in SARS-CoV-2 infection. *Neurobiol Dis* **168**, 105715 (2022).
10. D. Davalos *et al.*, ATP mediates rapid microglial response to local brain injury in vivo. *Nat Neurosci* **8**, 752-758 (2005).
11. A. Nimmerjahn, F. Kirchhoff, F. Helmchen, Resting microglial cells are highly dynamic surveillants of brain parenchyma in vivo. *Science* **308**, 1314-1318 (2005).
12. R. M. Ransohoff, V. H. Perry, Microglial physiology: unique stimuli, specialized responses. *Annu Rev Immunol* **27**, 119-145 (2009).
13. H. Wake, A. J. Moorhouse, S. Jinno, S. Kohsaka, J. Nabekura, Resting microglia directly monitor the functional state of synapses in vivo and determine the fate of ischemic terminals. *J Neurosci* **29**, 3974-3980 (2009).
14. M. E. Tremblay, R. L. Lowery, A. K. Majewska, Microglial interactions with synapses are modulated by visual experience. *PLoS Biol* **8**, e1000527 (2010).
15. K. M. Lucin, T. Wyss-Coray, Immune activation in brain aging and neurodegeneration: too much or too little? *Neuron* **64**, 110-122 (2009).
16. Q. Li, B. A. Barres, Microglia and macrophages in brain homeostasis and disease. *Nat Rev Immunol* **18**, 225-242 (2018).
17. D. P. Schafer, E. K. Lehrman, B. Stevens, The "quad-partite" synapse: microglia-synapse interactions in the developing and mature CNS. *Glia* **61**, 24-36 (2013).
18. D. J. Stein, M. F. Vasconcelos, L. Albrechet-Souza, K. M. M. Cereser, R. M. M. de Almeida, Microglial Over-Activation by Social Defeat Stress Contributes to Anxiety- and Depressive-Like Behaviors. *Front Behav Neurosci* **11**, 207 (2017).
19. U. B. Eyo *et al.*, Neuronal hyperactivity recruits microglial processes via neuronal NMDA receptors and microglial P2Y12 receptors after status epilepticus. *J Neurosci* **34**, 10528-10540 (2014).

20. A. M. Fontainhas *et al.*, Microglial morphology and dynamic behavior is regulated by ionotropic glutamatergic and GABAergic neurotransmission. *PLoS One* **6**, e15973 (2011).
21. Y. Li, X. F. Du, C. S. Liu, Z. L. Wen, J. L. Du, Reciprocal regulation between resting microglial dynamics and neuronal activity in vivo. *Dev Cell* **23**, 1189-1202 (2012).
22. J. Damas *et al.*, Broad host range of SARS-CoV-2 predicted by comparative and structural analysis of ACE2 in vertebrates. *Proc Natl Acad Sci U S A* **117**, 22311-22322 (2020).
23. M. A. A. Mahdy, W. Younis, Z. Ewaida, An Overview of SARS-CoV-2 and Animal Infection. *Front Vet Sci* **7**, 596391 (2020).
24. D. V. Glazkova *et al.*, Generation of SARS-CoV-2 Mouse Model by Transient Expression of the Human ACE2 Gene Mediated by Intranasal Administration of AAV-hACE2. *Mol Biol* **56**, 705-712 (2022).
25. J. Sun *et al.*, Generation of a Broadly Useful Model for COVID-19 Pathogenesis, Vaccination, and Treatment. *Cell* **182**, 734-743 e735 (2020).
26. J. Zheng *et al.*, COVID-19 treatments and pathogenesis including anosmia in K18-hACE2 mice. *Nature* **589**, 603-607 (2021).
27. L. R. Wong *et al.*, Eicosanoid signalling blockade protects middle-aged mice from severe COVID-19. *Nature* **605**, 146-151 (2022).
28. P. H. Janak, K. M. Tye, From circuits to behaviour in the amygdala. *Nature* **517**, 284-292 (2015).
29. L. R. Wong *et al.*, Sensitization of Non-permissive Laboratory Mice to SARS-CoV-2 with a Replication-Deficient Adenovirus Expressing Human ACE2. *STAR Protoc* **1**, 100169 (2020).
30. J. Du *et al.*, Transient acidosis while retrieving a fear-related memory enhances its lability. *Elife* **6** (2017).
31. G. Matute-Bello *et al.*, An official American Thoracic Society workshop report: features and measurements of experimental acute lung injury in animals. *Am J Respir Cell Mol Biol* **44**, 725-738 (2011).
32. F. Levet, J. Tonnesen, U. V. Nagerl, J. B. Sibarita, SpineJ: A software tool for quantitative analysis of nanoscale spine morphology. *Methods* **174**, 49-55 (2020).
33. C. J. Kreple *et al.*, Acid-sensing ion channels contribute to synaptic transmission and inhibit cocaine-evoked plasticity. *Nat Neurosci* **17**, 1083-1091 (2014).
34. W. J. Wright *et al.*, Silent synapses dictate cocaine memory destabilization and reconsolidation. *Nat Neurosci* **23**, 32-46 (2020).
35. H. Shuai *et al.*, Emerging SARS-CoV-2 variants expand species tropism to murines. *EBioMedicine* **73**, 103643 (2021).
36. F. Rigoli, M. Ewbank, T. Dalgleish, A. Calder, Threat visibility modulates the defensive brain circuit underlying fear and anxiety. *Neurosci Lett* **612**, 7-13 (2016).
37. J. Oh *et al.*, SARS-CoV-2 spike protein induces cognitive deficit and anxiety-like behavior in mouse via non-cell autonomous hippocampal neuronal death. *Sci Rep* **12**, 5496 (2022).

38. C.-Y. Chen, Y.-C. Chou, Y.-P. Hsueh, SARS-CoV-2 D614 and G614 spike variants impair neuronal synapses and exhibit differential fusion ability. *BioRxiv* 10.1101/2020.12.03.409763 (2020).
39. M. G. Frank *et al.*, SARS-CoV-2 spike S1 subunit induces neuroinflammatory, microglial and behavioral sickness responses: Evidence of PAMP-like properties. *Brain Behav Immun* **100**, 267-277 (2022).
40. G. Datta *et al.*, SARS-CoV-2 S1 Protein Induces Endolysosome Dysfunction and Neuritic Dystrophy. *Front Cell Neurosci* **15**, 777738 (2021).
41. S. Zhang *et al.*, Resveratrol Attenuates Microglial Activation via SIRT1-SOCS1 Pathway. *Evid Based Complement Alternat Med* **2017**, 8791832 (2017).
42. K. M. Woolfrey, D. P. Srivastava, Control of Dendritic Spine Morphological and Functional Plasticity by Small GTPases. *Neural Plast* **2016**, 3025948 (2016).
43. G. Yang, F. Pan, W. B. Gan, Stably maintained dendritic spines are associated with lifelong memories. *Nature* **462**, 920-924 (2009).
44. J. N. Bourne, K. M. Harris, Balancing structure and function at hippocampal dendritic spines. *Annu Rev Neurosci* **31**, 47-67 (2008).
45. C. H. Bailey, E. R. Kandel, K. M. Harris, Structural Components of Synaptic Plasticity and Memory Consolidation. *Cold Spring Harb Perspect Biol* **7**, a021758 (2015).
46. A. Peters, I. R. Kaiserman-Abramof, The small pyramidal neuron of the rat cerebral cortex. The perikaryon, dendrites and spines. *Am J Anat* **127**, 321-355 (1970).
47. K. P. Berry, E. Nedivi, Spine Dynamics: Are They All the Same? *Neuron* **96**, 43-55 (2017).
48. E. E. Koffman *et al.*, Acid-sensing ion channel 1a regulates the specificity of reconsolidation of conditioned threat responses. *JCI Insight* 10.1172/jci.insight.155341 (2022).
49. A. Vidal-Itriago *et al.*, Microglia morphophysiological diversity and its implications for the CNS. *Front Immunol* **13**, 997786 (2022).
50. M. Colonna, O. Butovsky, Microglia Function in the Central Nervous System During Health and Neurodegeneration. *Annu Rev Immunol* **35**, 441-468 (2017).
51. S.-S. Lin, Y. Tang, P. Illes, A. Verkhratsky, The Safeguarding Microglia: Central Role for P2Y12 Receptors. *Frontiers in Pharmacology* **11** (2021).
52. L. J. Wu, K. I. Vadakkan, M. Zhuo, ATP-induced chemotaxis of microglial processes requires P2Y receptor-activated initiation of outward potassium currents. *Glia* **55**, 810-821 (2007).
53. R. D. Fields, Nonsynaptic and nonvesicular ATP release from neurons and relevance to neuron-glia signaling. *Semin Cell Dev Biol* **22**, 214-219 (2011).
54. R. Luu *et al.*, Pannexin-1 channel opening is critical for COVID-19 pathogenesis. *iScience* **24**, 103478 (2021).
55. D. E. Ribeiro *et al.*, Hyperactivation of P2X7 receptors as a culprit of COVID-19 neuropathology. *Mol Psychiatry* **26**, 1044-1059 (2021).
56. S. M. Burks, H. Rosas-Hernandez, M. Alejandro Ramirez-Lee, E. Cuevas, J. C. Talpos, Can SARS-CoV-2 infect the central nervous system via the olfactory bulb or the blood-brain barrier? *Brain Behav Immun* **95**, 7-14 (2021).

57. K. Tomonaga, Virus-induced neurobehavioral disorders: mechanisms and implications. *Trends Mol Med* **10**, 71-77 (2004).
58. I. Kotsiri *et al.*, Viral Infections and Schizophrenia: A Comprehensive Review. *Viruses* **15** (2023).
59. M. E. Tremblay, C. Madore, M. Bordeleau, L. Tian, A. Verkhratsky, Neuropathobiology of COVID-19: The Role for Glia. *Front Cell Neurosci* **14**, 592214 (2020).
60. D. Beckman *et al.*, SARS-CoV-2 infects neurons and induces neuroinflammation in a non-human primate model of COVID-19. *Cell Rep* **41**, 111573 (2022).
61. S. J. Rhie, E. Y. Jung, I. Shim, The role of neuroinflammation on pathogenesis of affective disorders. *J Exerc Rehabil* **16**, 2-9 (2020).
62. N. Vogelzangs, P. de Jonge, J. H. Smit, S. Bahn, B. W. Penninx, Cytokine production capacity in depression and anxiety. *Transl Psychiatry* **6**, e825 (2016).
63. M. Schafers, L. Sorkin, Effect of cytokines on neuronal excitability. *Neurosci Lett* **437**, 188-193 (2008).
64. S. Rossi *et al.*, Interleukin-1beta causes anxiety by interacting with the endocannabinoid system. *J Neurosci* **32**, 13896-13905 (2012).
65. R. K. Farooq, K. Asghar, S. Kanwal, A. Zulqernain, Role of inflammatory cytokines in depression: Focus on interleukin-1beta. *Biomed Rep* **6**, 15-20 (2017).
66. M. A. Alshammari *et al.*, Systemic TNF-alpha blockade attenuates anxiety and depressive-like behaviors in db/db mice through downregulation of inflammatory signaling in peripheral immune cells. *Saudi Pharm J* **28**, 621-629 (2020).
67. J. Qin, Z. Ma, X. Chen, S. Shu, Microglia activation in central nervous system disorders: A review of recent mechanistic investigations and development efforts. *Front Neurol* **14**, 1103416 (2023).
68. Y. Ma *et al.*, Long-Term Consequences of Asymptomatic SARS-CoV-2 Infection: A Systematic Review and Meta-Analysis. *Int J Environ Res Public Health* **20** (2023).
69. E. M. Gibson *et al.*, Methotrexate Chemotherapy Induces Persistent Tri-glial Dysregulation that Underlies Chemotherapy-Related Cognitive Impairment. *Cell* **176**, 43-55 e13 (2019).
70. M. L. Monje, S. Mizumatsu, J. R. Fike, T. D. Palmer, Irradiation induces neural precursor-cell dysfunction. *Nat Med* **8**, 955-962 (2002).
71. M. L. Monje, H. Toda, T. D. Palmer, Inflammatory blockade restores adult hippocampal neurogenesis. *Science* **302**, 1760-1765 (2003).
72. M. L. Monje *et al.*, Impaired human hippocampal neurogenesis after treatment for central nervous system malignancies. *Ann Neurol* **62**, 515-520 (2007).
73. A. Fernandez-Castaneda *et al.*, Mild respiratory COVID can cause multi-lineage neural cell and myelin dysregulation. *Cell* **185**, 2452-2468 e2416 (2022).

Figure. 1

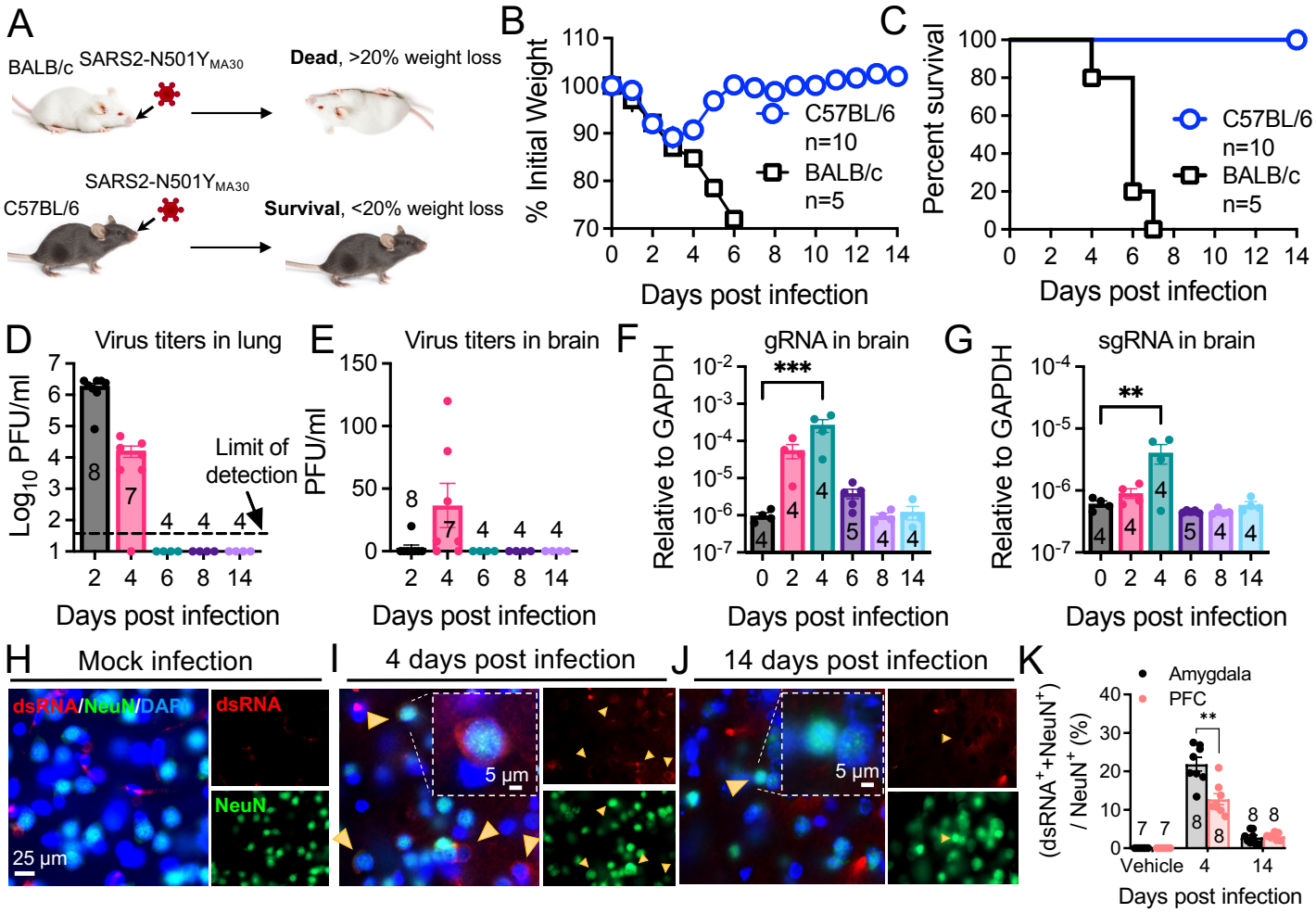
A
BALB/c SARS2-N501Y$_{MA30}$
Dead, >20% weight loss
SARS2-N501Y$_{MA30}$
C57BL/6
Survival, <20% weight loss
B
% Initial Weight
C57BL/6 n=10
BALB/c n=5
Days post infection
C
Percent survival
C57BL/6 n=10
BALB/c n=5
Days post infection
D
Virus titers in lung
Log$_{10}$ PFU/ml
Limit of detection
Days post infection
E
Virus titers in brain
PFU/ml
Days post infection
F
gRNA in brain
Relative to GAPDH
***
Days post infection
G
sgRNA in brain
Relative to GAPDH
**
Days post infection
H
Mock infection
dsRNA/NeuN/DAPI
dsRNA
NeuN
25 μm
I
4 days post infection
5 μm
J
14 days post infection
5 μm
K
Amygdala
PFC
(dsRNA$^+$+NeuN$^+$) / NeuN$^+$ (%)
**
Vehicle
Days post infection

Figure. 2

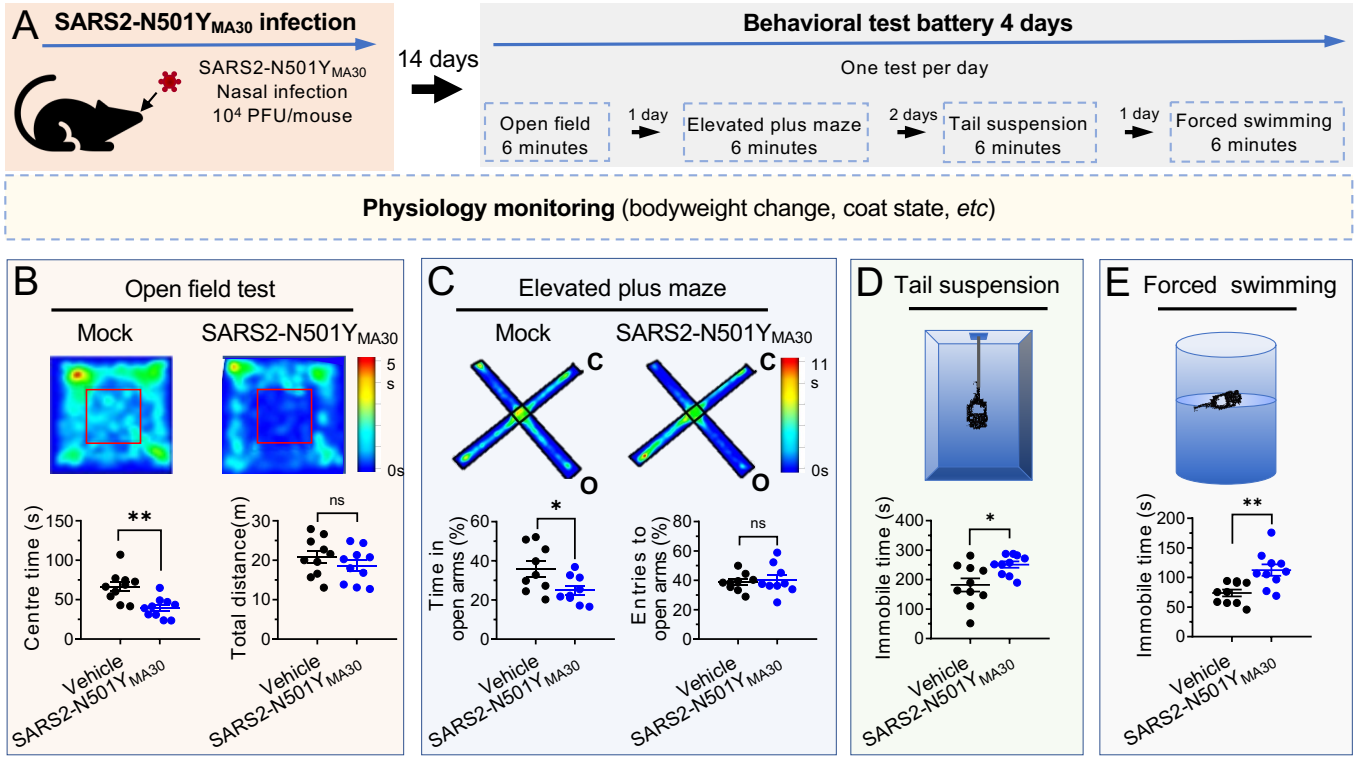
A
SARS2-N501Y$_{MA30}$ infection
SARS2-N501Y$_{MA30}$
Nasal infection
10^4 PFU/mouse
14 days
Behavioral test battery 4 days
One test per day
Open field
6 minutes
1 day
Elevated plus maze
6 minutes
2 days
Tail suspension
6 minutes
1 day
Forced swimming
6 minutes
Physiology monitoring (bodyweight change, coat state, etc)
B
Open field test
Mock
SARS2-N501Y$_{MA30}$
5
s
0s
Centre time (s)
Total distance(m)
ns
Vehicle
SARS2-N501Y$_{MA30}$
C
Elevated plus maze
Mock
SARS2-N501Y$_{MA30}$
C
O
11
s
0s
Time in open arms (%)
Entries to open arms (%)
ns
Vehicle
SARS2-N501Y$_{MA30}$
D
Tail suspension
Immobile time (s)
Vehicle
SARS2-N501Y$_{MA30}$
E
Forced swimming
Immobile time (s)
Vehicle
SARS2-N501Y$_{MA30}$

Figure. 3

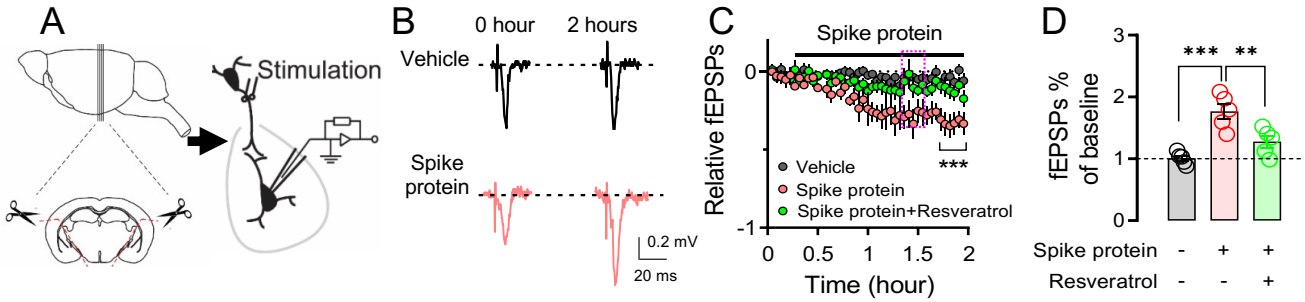
A
Stimulation
B
0 hour
2 hours
Vehicle
Spike protein
0.2 mV
20 ms
C
Spike protein
Relative fEPSPs
Vehicle
Spike protein
Spike protein+Resveratrol
***
Time (hour)
D
fEPSPs % of baseline
***
**
Spike protein
Resveratrol

Figure. 4

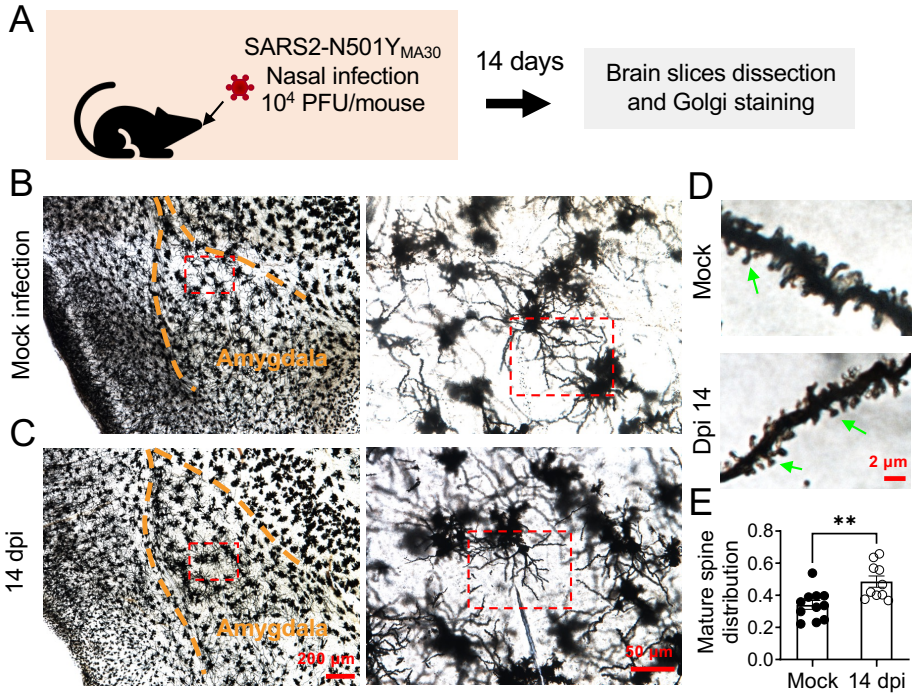
A
SARS2-N501Y$_{MA30}$
Nasal infection
10^4 PFU/mouse
14 days
Brain slices dissection
and Golgi staining
B
Mock infection
Amygdala
C
14 dpi
Amygdala
200 μm
50 μm
D
Mock
Dpi 14
2 μm
E
Mature spine distribution
0.8
0.6
0.4
0.2
0.0
**
Mock
14 dpi

Figure. 5

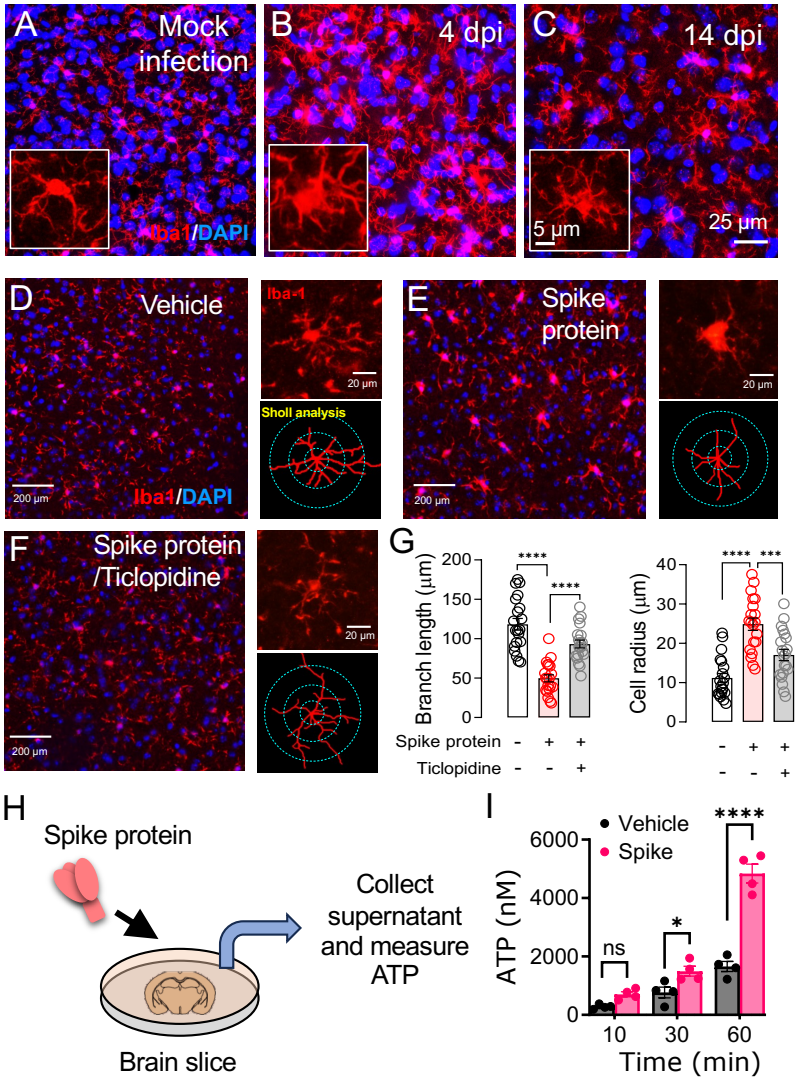
A
Mock infection
Iba1/DAPI
B
4 dpi
C
14 dpi
5 μm
25 μm
D
Vehicle
Iba-1
20 μm
Sholl analysis
200 μm
Iba1/DAPI
E
Spike protein
F
Spike protein /Ticlopidine
G
Branch length (μm)
Cell radius (μm)
Spike protein
Ticlopidine
H
Spike protein
Collect supernatant and measure ATP
Brain slice
I
Vehicle
Spike
ATP (nM)
ns
Time (min)

Figure. 6

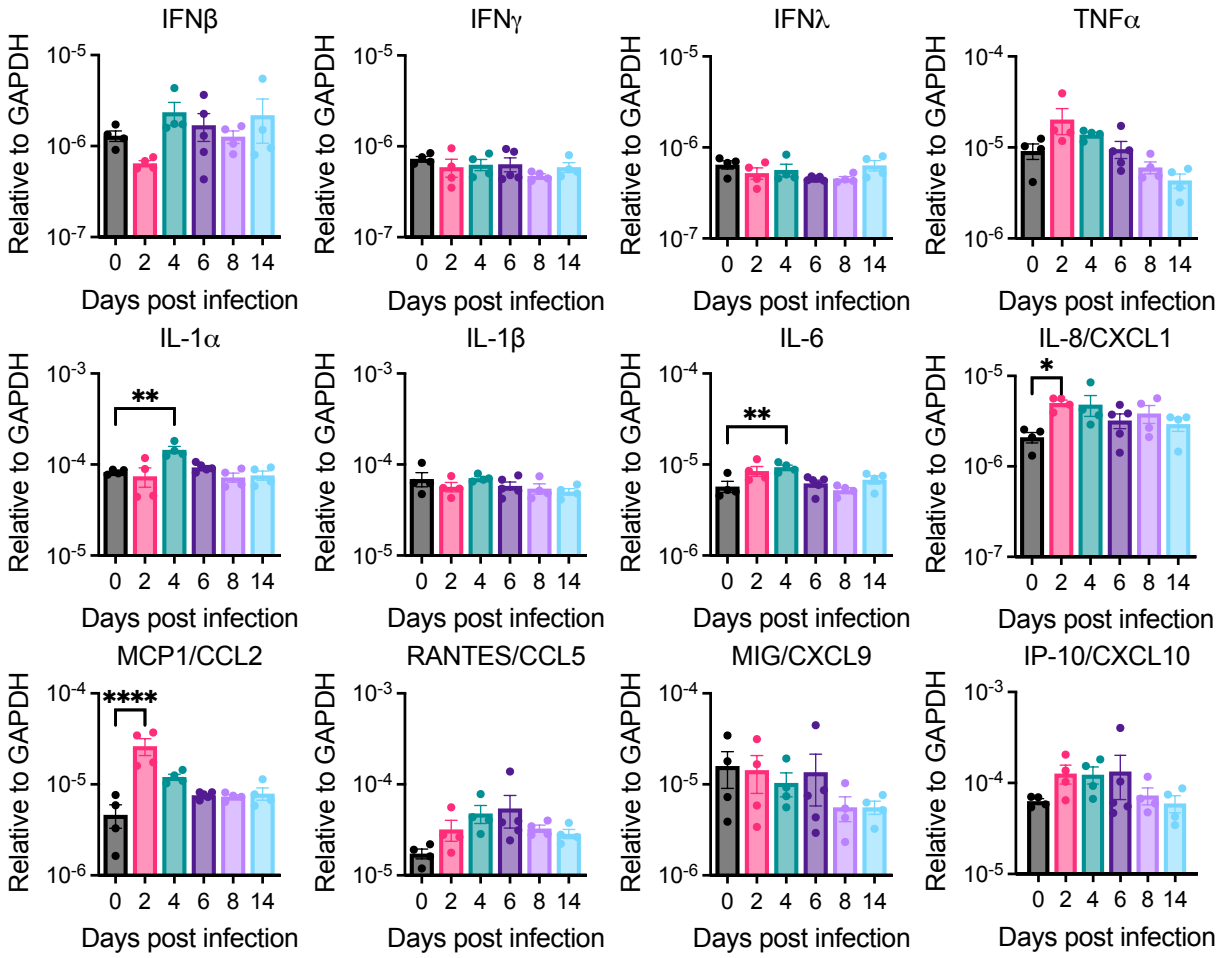
IFNβ
IFNγ
IFNλ
TNFα
IL-1α
IL-1β
IL-6
IL-8/CXCL1
MCP1/CCL2
RANTES/CCL5
MIG/CXCL9
IP-10/CXCL10
Relative to GAPDH
Days post infection
0 2 4 6 8 14
**
*
****

Figure. 7

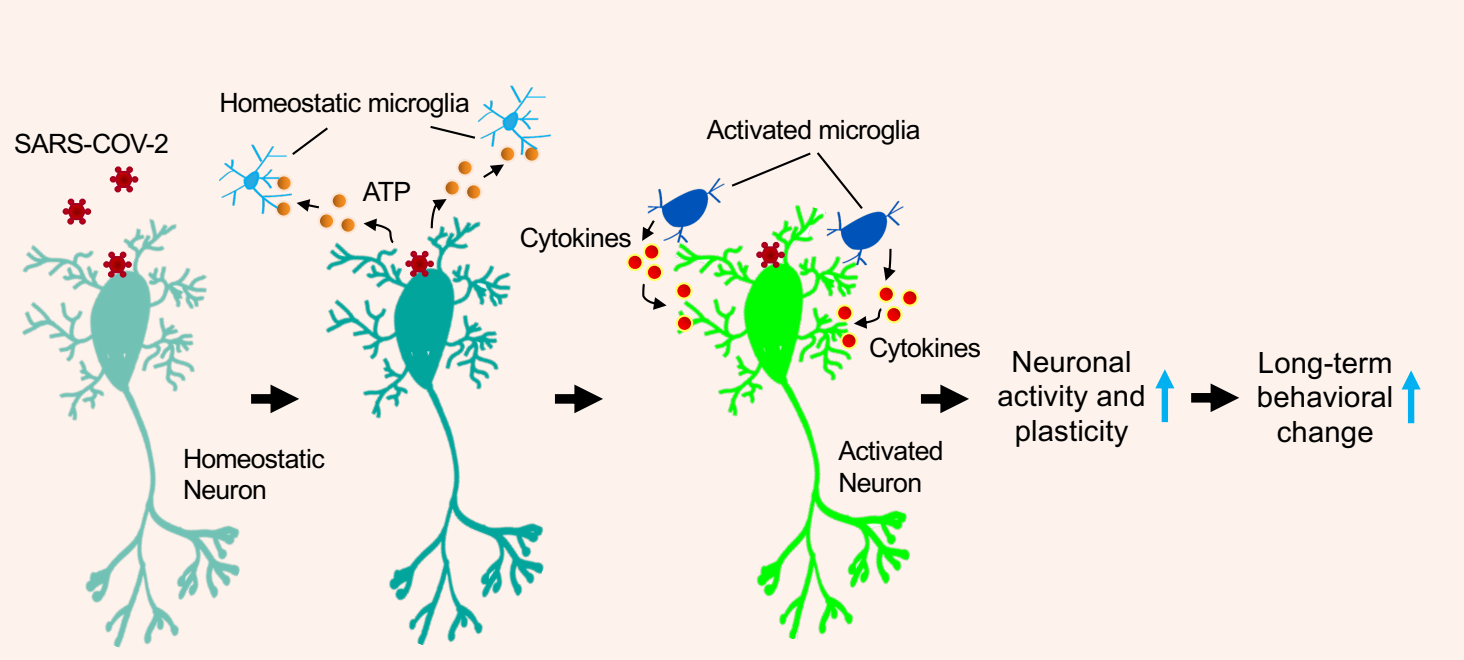
SARS-COV-2
Homeostatic microglia
ATP
Homeostatic
Neuron
Activated microglia
Cytokines
Cytokines
Activated
Neuron
Neuronal
activity and
plasticity
Long-term
behavioral
change

Supple Figure. 1

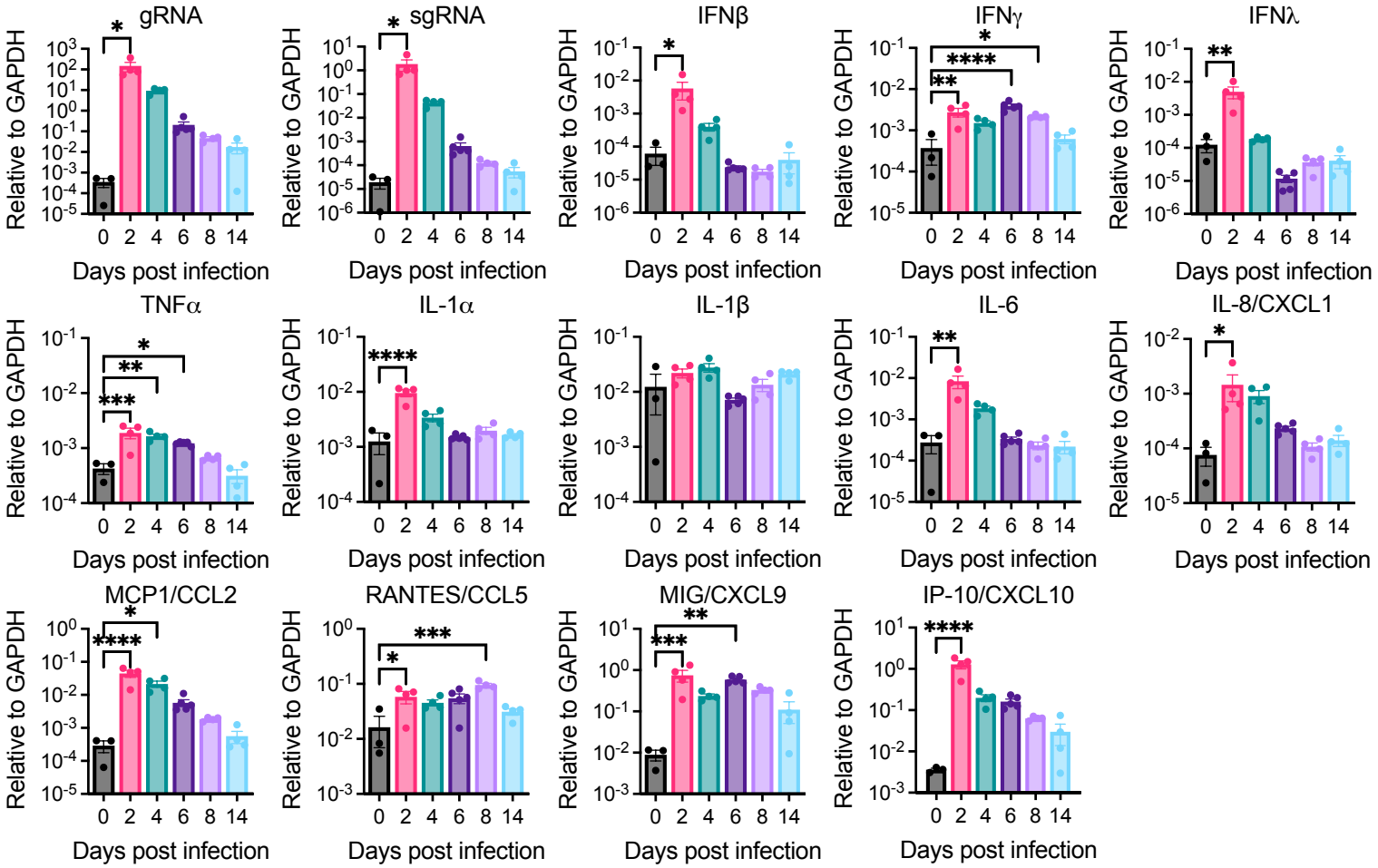

Supple Figure. 2

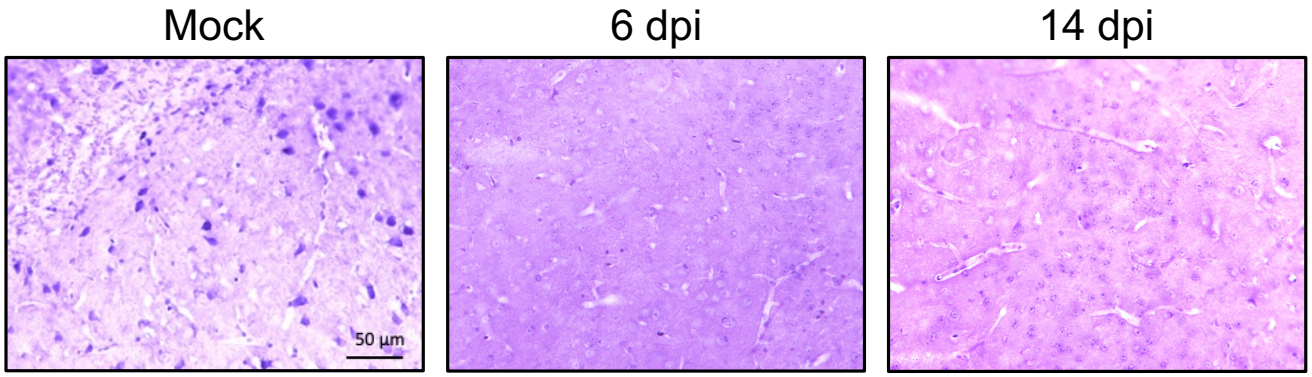

Supple Figure. 3

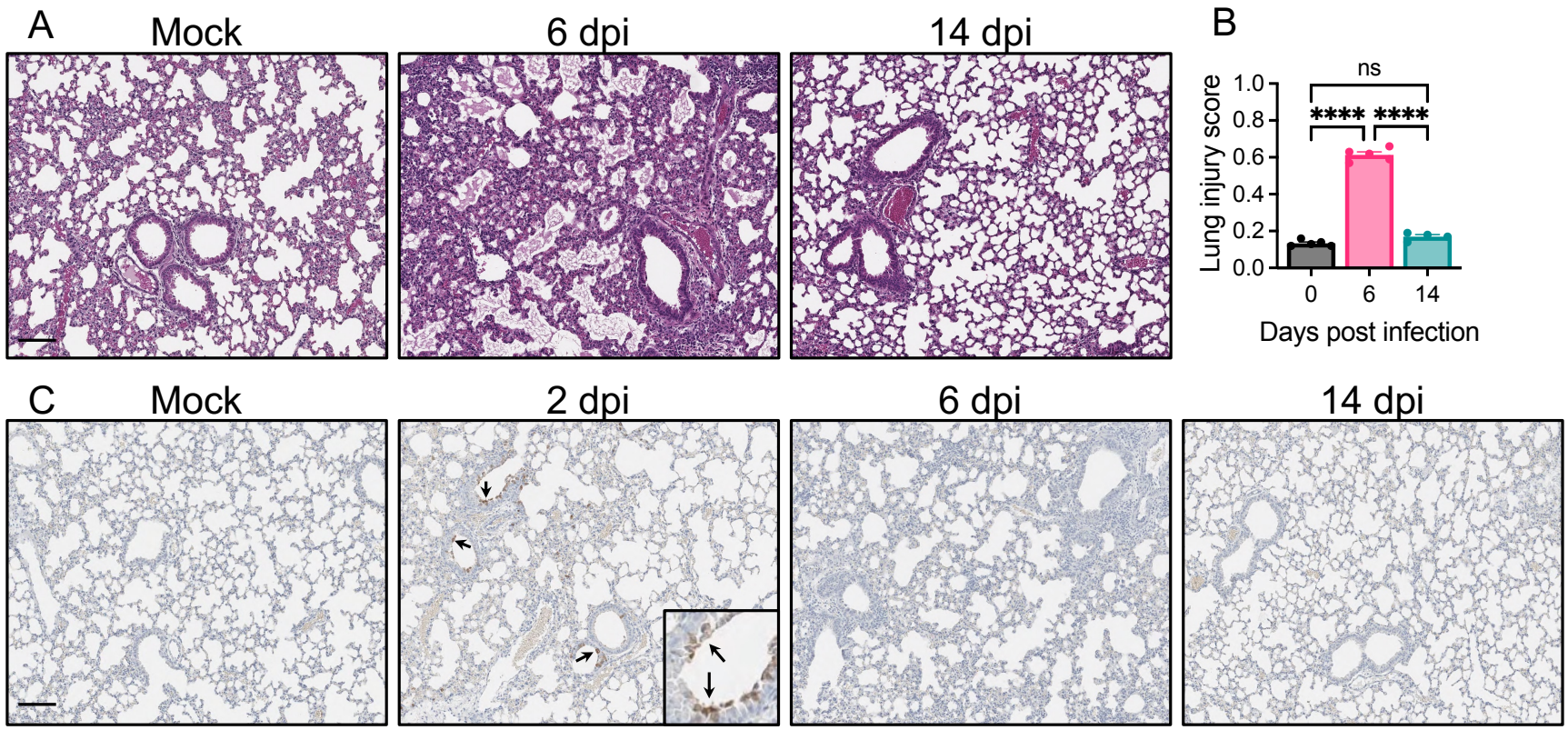

S1 Table. Quantitative real-time PCR analysis of viral RNA

Gene	Forward Primer	Reverse Primer
2019-nCoV_N1	GACCCCAAAATCAGCGAAAT	TCTGGT TACTGCCAGTTGAATCTG
SARS-CoV-2 sgRNA for E	CGATCTCTTGTAGATCTGTTCTC	ATATTGCAGCAGTACGCACACA
mGAPDH	AACAGCAACTCCCACTCTTC	CCTGTTGCTGTAGCCGTATT
mIFNβ	TCAGAATGAGTGGTGGTTGC	GACCTTTCAAATGCAGTAGATTCA
mIFNγ	CGGCACAGTCATTGAAAGCCTA	GTTGCTGATGGCCTGATTGTC
mIFNλ	AGCTGCAGGTCCAAGAGCG	GGTGGTCAGGGCTGAGTCATT
mTNFα	GAACTGGCAGAAGAGGCACT	AGGGTCTGGGCCATAGAACT
mIL1a	CGCTTGAGTCGGCAAAGAAAT	ACAAACTGATCTGTGCAAGTCTC
mIL-1b	ACTGTTTCTAATGCCTTCCC	ATGGTTTCTTGTGACCCTGA
mIL-6	GAGGATACCACTCCCAACAGACC	AAGTGCATCATCGTTGTTCATACA
mIL-8	CACCTCAAGAACATCCAGAGCT	CAAGCAGAACTGAACTACCATCG
mCCL2	CTTCTGGGCCTGCTGTTCA	CCAGCCTACTCATTGGGATCA
mCCL5	AGATCTCTGCAGCTGCCCTCA	GGAGCACTTGCTGCTGGTGTAG
mCXCL9	GCCATGAAGTCCGCTGTTCT	GGGTTCCTCGAACTCCACACT
mCXCL10	GCCGTCATTTTCTGCCTCAT	GCTTCCCTATGGCCCTCATT